Commun. Comput. Phys.
doi: 10.4208/cicp.OA-2019-0163

Vol. **27**, No. 5, pp. 1530-1549
May 2020

# Improved RBF Collocation Methods for Fourth Order Boundary Value Problems

C. S. Chen[1], Andreas Karageorghis[2] and Hui Zheng[3,*]

[1] *School of Civil Engineering and Architecture, Nanchang University, Nanchang, China, and School of Mathematics and Natural Sciences, University of Southern Mississippi, Hattiesburg, MS 39406, USA.*
[2] *Department of Mathematics and Statistics, University of Cyprus/* Πανεπιστήμιο Κύπρου, *P.O. Box 20537, 1678 Nicosia/*Λευκωσία, *Cyprus/*Κύπρος.
[3] *School of Civil Engineering and Architecture, Nanchang University, Nanchang, China.*

Received 23 September 2019; Accepted (in revised version) 16 October 2019

**Abstract.** Radial basis function (RBF) collocation methods (RBFCMs) are applied to fourth order boundary value problems (BVPs). In particular, we consider the classical Kansa method and the method of approximate particular solutions (MAPS). In the proposed approach we include some so-called ghost points which are located inside and outside the domain of the problem. The inclusion of these points is shown to improve the accuracy and the stability of the collocation methods. An appropriate value of the shape parameter in the RBFs used is obtained using either the leave-one-out cross validation (LOOCV) algorithm or Franke's formula. We present and analyze the results of several numerical tests.

**AMS subject classifications**: 65N35, 65N99

**Key words**: Radial basis functions, Kansa method, method of particular solutions, collocation, fourth order PDEs.

## 1 Introduction

In recent years, meshless methods have undergone vigorous development and have matured as methods of choice for the solution of various science and engineering problems. Unlike other traditional mesh-based methods such as the finite element method [1,2,25], the finite difference method [34,35], and the finite volume method [22,23], the main attraction of meshless methods is their ability to easily and effectively solve problems in

*Corresponding author. *Email addresses:* zhenghui@ncu.edu.cn (H. Zheng), cs.chen@usm.edu (C. S. Chen), andreask@ucy.ac.cy (A. Karageorghis)

 

complex geometries, particularly in high dimensions. There are various types of meshless methods and among them, radial basis function (RBF) collocation methods (RBFCMs) have become increasingly popular and attracted considerable attention in recent years for solving partial differential equations (PDEs). The first RBFCM was proposed by Kansa in 1990 [17] and, over the years, various kinds of RBFCMs, such as the method of approximate particular solutions (MAPS) [3], the RBF-differential quadrature method [32], collocation for Cauchy problems [24], and the RBF Hermite collocation method [8], have been proposed. Note that each of the above RBFCMs has its own advantages and disadvantages. Undoubtedly, the most famous and popular RBFCM is the Kansa method which we shall be investigating in the current study. The Kansa method is known to produce highly accurate results but is sensitive to the RBF shape parameter values and its stability can be an issue. Among all of the above RBFCMs, the MAPS is an alternative indirect method closely related to the Kansa method and has also proved to be effective. Unlike the Kansa method, the MAPS adopts a particular solution of the considered differential operator, with respect to the RBF, as the "new" basis function. The derivation of a particular solution comes from an integration process and the obtained approximation is usually more stable with respect to the shape parameter. In the last few years, the MAPS has attracted some attention in the RBF community and has been applied to solve a large class of PDEs. Despite the success of the MAPS, the derivation of a particular solution in closed-form for general differential operators remains a major challenge. For high order differential operators, the derivation of a closed-form particular solution is substantially more difficult to obtain. Once the closed-form particular solution for a given basis function and differential operator is available, the MAPS converts the given PDE into an interpolation problem. Due to the difficulty of deriving a particular solution for a general differential operator, an alternative is the use of the particular solution of the Laplace operator for second order PDEs and the biharmonic operator for fourth order PDEs, as the basis function. This approach for solving fourth order PDEs will be adopted in this paper. It should be mentioned that often, in order to save computational effort in problems requiring a large number of nodes, global RBFs may be replaced by local RBF methods [4, 6, 21, 38].

A major challenge in RBFCMs is the determination of an optimal, or at least suitable, value of the shape parameter in the RBF used. Various studies have attempted to overcome this difficulty, see, for example, [16, 18, 19, 29]. We shall use the leave-one-out cross validation algorithm (LOOCV) [10, 29] and a modification of Franke's formula [12]. The issue of determining an appropriate value of the shape parameter can be avoided by using polyharmonic splines with additional polynomials which gives comparable accuracy to infinitely differentiable RBFs, see, e.g. [11, 16, 28, 37].

Fourth order boundary value problems (BVPs) are important in modelling various types of physical problems such as plate bending [13], fluid dynamics [15], and computer graphics problems [33], to name a few. Many meshless methods have been developed for the solution of fourth order PDEs where one of the challenges is that two boundary conditions need to be imposed. As such, the resulting matrix in the classical

RBFCM is non-square and the overall accuracy and stability of the numerical results are somehow affected. In the current study we include a number of *ghost points* (or fictitious points) inside and outside the domain. The idea of using centres outside the domain of the problem under consideration is not new, see, e.g., [9, Chapter 39] and [20]. In these studies, the purpose of taking centres outside the domain is to compensate for the fact that the governing equation is also satisfied at the boundary points. These additional centres are placed close to the boundary and the improvement in the accuracy is only slight. As a result, this idea did not attract much further attention. Additional centres close to the boundary were also used in [31] to compensate for multiple boundary conditions in higher order PDEs. In our approach, the placement of the centres is very different and, as we shall see, the improvement in accuracy is quite high. These ghost points are considered as an extension of the boundary points which are floating around the domain. As a result, the discretization matrix becomes square and the stability and accuracy improve considerably. The presence of these ghost points is reminiscent of the presence of the sources in the method of fundamental solutions (MFS) [7, 14] where these points have to be located outside the domain. In our proposed approach, the ghost points may be also located inside the domain as long as they do not coincide with any interior or boundary points. In this study, we propose the deployment of the ghost points to improve the performance of the Kansa method and the MAPS for the solution of fourth order PDEs. The main distinction of our approach is the distribution of the ghost points not just on a curve in 2D or a surface in 3D close to the boundary as in [20, 31] but also inside and outside the domain. Furthermore, in order to achieve high accuracy, these ghost points need to be distributed randomly and far from the domain.

The paper is organized in the following way. In Section 2 we recall the Kansa method and the MAPS for solving second order BVPs and then describe its natural extension to fourth order BVPs with the addition of ghost points. The results of some numerical examples in 2D and 3D are presented and analyzed in Section 3. Some concluding remarks and areas of possible future investigations are given in Section 4.

## 2 RBF collocation methods

### 2.1 Second order problems

We recall the BVP in $\mathbb{R}^d$, $d=2$ or 3 consisting of the second order linear elliptic PDE

$$\mathcal{L}u = f \quad \text{in the domain } \Omega, \tag{2.1a}$$

and the linear boundary condition

$$\mathcal{B}u = g \quad \text{on the boundary } \partial\Omega. \tag{2.1b}$$

The numerical solution of such problems by RBF collocation methods is well-documented, see e.g. [9, 37]. Typically, the approximation of the solution of a BVP is

approximated by a taking a linear combination of RBFs $\phi_{\mathsf{n}}(x,y)$, $\mathsf{n}=1,\cdots,\mathsf{N}$, which have the form

$$\phi_{\mathsf{n}}(x,y)=\Phi(r_{\mathsf{n}}),\quad \text{where}\quad r_{\mathsf{n}}^2=(x-\mathrm{x}_{\mathsf{n}})^2+(y-\mathrm{y}_{\mathsf{n}})^2. \tag{2.2}$$

Each RBF $\phi_{\mathsf{n}}$ is linked to a point $(\mathrm{x}_{\mathsf{n}},\mathrm{y}_{\mathsf{n}})$. These points $\{(\mathrm{x}_{\mathsf{n}},\mathrm{y}_{\mathsf{n}})\}_{\mathsf{n}=1}^{\mathsf{N}}$ are the *centers*. We select $\mathsf{N}_{\mathsf{i}}$ interior centres $\{(\mathrm{x}_{\mathsf{n}},\mathrm{y}_{\mathsf{n}})\}_{\mathsf{n}=1}^{\mathsf{N}_{\mathsf{i}}}$ and $\mathsf{N}_{\mathsf{b}}$ boundary centres $\{(\mathrm{x}_{\mathsf{n}},\mathrm{y}_{\mathsf{n}})\}_{\mathsf{n}=\mathsf{N}_{\mathsf{i}}+1}^{\mathsf{N}_{\mathsf{i}}+\mathsf{N}_{\mathsf{b}}}$ and we take $\mathsf{N}=\mathsf{N}_{\mathsf{i}}+\mathsf{N}_{\mathsf{b}}$. Many RBFs include a *shape parameter*, which we shall denote by $c$. Determining the optimal value of the shape parameter is a major difficulty.

We shall use the Kansa method [17], in which the approximation of the solution of BVP (2.1) is

$$\hat{u}(x,y)=\sum_{\mathsf{n}=1}^{\mathsf{N}}a_{\mathsf{n}}\phi_{\mathsf{n}}(x,y),\qquad (x,y)\in\overline{\Omega}. \tag{2.3}$$

We also provide the *collocation points* $\{(x_{\mathsf{m}},y_{\mathsf{m}})\}_{\mathsf{m}=1}^{\mathsf{M}}\in\overline{\Omega}$ and select $\mathsf{M}_{\mathsf{i}}$ interior points $\{(x_{\mathsf{m}},y_{\mathsf{m}})\}_{\mathsf{m}=1}^{\mathsf{M}_{\mathsf{i}}}$ and $\mathsf{M}_{\mathsf{b}}$ boundary points $\{(x_{\mathsf{m}},y_{\mathsf{m}})\}_{\mathsf{m}=\mathsf{M}_{\mathsf{i}}+1}^{\mathsf{M}_{\mathsf{i}}+\mathsf{M}_{\mathsf{b}}}$. We take $\mathsf{M}=\mathsf{M}_{\mathsf{i}}+\mathsf{M}_{\mathsf{b}}$. It should be noted that approximation (2.3) may, in some cases, be augmented by some polynomial basis functions.

Often, we take fewer centres than collocation points.

We determine the coefficients $\{a_{\mathsf{n}}\}_{\mathsf{n}=1}^{\mathsf{N}}$ in Eq. (2.3) from the equations

$$\mathcal{L}\hat{u}(x_{\mathsf{m}},y_{\mathsf{m}})=f(x_{\mathsf{m}},y_{\mathsf{m}}),\quad \mathsf{m}=1,\cdots,\mathsf{M}_{\mathsf{i}}, \tag{2.4a}$$

$$\mathcal{B}\hat{u}(x_{\mathsf{m}},y_{\mathsf{m}})=g(x_{\mathsf{m}},y_{\mathsf{m}}),\quad \mathsf{m}=\mathsf{M}_{\mathsf{i}}+1,\cdots,\mathsf{M}_{\mathsf{i}}+\mathsf{M}_{\mathsf{b}}. \tag{2.4b}$$

As there are $\mathsf{M}$ equations in $\mathsf{N}$ unknowns $\boldsymbol{a}=[a_1,a_2,\cdots,a_{\mathsf{N}}]^T$, we choose $\mathsf{M}\geq\mathsf{N}$.

The above equations yield the $\mathsf{M}\times\mathsf{N}$ linear system

$$\left(\frac{A_{\mathcal{L}}}{A_{\mathcal{B}}}\right)\begin{pmatrix}a_1\\a_2\\\vdots\\a_{\mathsf{N}}\end{pmatrix}=\left(\frac{\boldsymbol{f}}{\boldsymbol{g}}\right), \tag{2.5}$$

where $\boldsymbol{f}=[f_1,f_2,\cdots,f_{\mathsf{M}_{\mathsf{i}}}]$ with $f_m=f(x_{\mathsf{m}},y_{\mathsf{m}})$, $\mathsf{m}=1,\cdots,\mathsf{M}_{\mathsf{i}}$, and $\boldsymbol{g}=[g_1,g_2,\cdots,g_{\mathsf{M}_{\mathsf{b}}}]$ with $g_\ell=g(x_{\mathsf{M}_{\mathsf{i}}+\ell},y_{\mathsf{M}_{\mathsf{i}}+\ell})$, $\ell=1,\cdots,\mathsf{M}_{\mathsf{b}}$.

In addition,

$$A_{\mathcal{L}}\in\mathbb{R}^{\mathsf{M}_{\mathsf{i}}\times\mathsf{N}},\quad \text{where}\quad (A_{\mathcal{L}})_{\mathsf{m},\mathsf{n}}=\mathcal{L}\phi_{\mathsf{n}}(x_{\mathsf{m}},y_{\mathsf{m}}),\ \ \mathsf{m}=1,\cdots,\mathsf{M}_{\mathsf{i}},\ \ \mathsf{n}=1,\cdots,\mathsf{N},$$

and

$$A_{\mathcal{B}}\in\mathbb{R}^{\mathsf{M}_{\mathsf{b}}\times\mathsf{N}},\quad \text{where}\quad (A_{\mathcal{B}})_{\ell,\mathsf{n}}=\mathcal{B}\phi_{\mathsf{n}}(x_{\mathsf{M}_{\mathsf{i}}+\ell},y_{\mathsf{M}_{\mathsf{i}}+\ell}),\ \ \ell=1,\cdots,\mathsf{M}_{\mathsf{b}},\ \ \mathsf{n}=1,\cdots,\mathsf{N}.$$

When the centres and the collocation points are the same, system (2.5) becomes square.

## 2.2 Fourth order problems

We now consider the BVP in $\mathbb{R}^{\mathrm{d}}$, $\mathrm{d}=2$ or 3 consisting of the fourth order linear elliptic PDE

$$\mathcal{L}u=f \quad \text{in the domain } \Omega, \tag{2.6a}$$

and the linear boundary conditions

$$\mathcal{B}_1 u=g \quad \text{and} \quad \mathcal{B}_2 u=h \quad \text{on the boundary } \partial\Omega. \tag{2.6b}$$

For fourth order problems, we shall consider the case when the collocation points and centre points are the same. Hence, we consider the interior centres/collocation points $\{(\mathrm{x_n},\mathrm{y_n})\}_{\mathrm{n}=1}^{\mathrm{N_i}}$ and the boundary centres/collocation points $\{(\mathrm{x_n},\mathrm{y_n})\}_{\mathrm{n}=\mathrm{N_i}+1}^{\mathrm{N_i}+\mathrm{N_b}}$. The total number of centres/collocation points is thus $\mathrm{N}=\mathrm{N_i}+\mathrm{N_b}$.

### 2.2.1 The Kansa method

In the Kansa method the solution of BVP (2.6) is approximated by

$$\hat{u}(x,y)=\sum_{\mathrm{n}=1}^{\mathrm{N}} a_{\mathrm{n}}\phi_{\mathrm{n}}(x,y), \qquad (x,y)\in\overline{\Omega}. \tag{2.7}$$

The coefficients $\{a_{\mathrm{n}}\}_{\mathrm{n}=1}^{\mathrm{N}}$ are obtained from the equations

$$\mathcal{L}\hat{u}(x_{\mathrm{m}},y_{\mathrm{m}})=f(x_{\mathrm{m}},y_{\mathrm{m}}), \quad \mathrm{m}=1,\cdots,\mathrm{N_i}, \tag{2.8a}$$
$$\mathcal{B}_1\hat{u}(x_{\mathrm{m}},y_{\mathrm{m}})=g(x_{\mathrm{m}},y_{\mathrm{m}}), \quad \mathrm{m}=\mathrm{N_i}+1,\cdots,\mathrm{N_i}+\mathrm{N_b}, \tag{2.8b}$$
$$\mathcal{B}_2\hat{u}(x_{\mathrm{m}},y_{\mathrm{m}})=h(x_{\mathrm{m}},y_{\mathrm{m}}), \quad \mathrm{m}=\mathrm{N_i}+1,\cdots,\mathrm{N_i}+\mathrm{N_b}. \tag{2.8c}$$

The above equations yield the over-determined $(\mathrm{N}+\mathrm{N_b})\times\mathrm{N}$ linear system

$$\left(\begin{array}{c} A_{\mathcal{L}} \\ \hline A_{\mathcal{B}_1} \\ \hline A_{\mathcal{B}_2} \end{array}\right)\begin{pmatrix} a_1 \\ a_2 \\ \vdots \\ a_{\mathrm{N}} \end{pmatrix}=\left(\begin{array}{c} \boldsymbol{f} \\ \hline \boldsymbol{g} \\ \hline \boldsymbol{h} \end{array}\right), \tag{2.9}$$

where the vectors $\boldsymbol{f}$ and $\boldsymbol{g}$ are defined as in (2.5) and $\boldsymbol{h}=[h_1,h_2,\cdots,h_{\mathrm{N_b}}]$ with $h_\ell=h(x_{\mathrm{N_i}+\ell},y_{\mathrm{N_i}+\ell})$, $\ell=1,\cdots,\mathrm{N_b}$.

In addition,

$$A_{\mathcal{L}}\in\mathbb{R}^{\mathrm{N_i}\times\mathrm{N}}, \quad \text{where} \quad (A_{\mathcal{L}})_{\mathrm{m,n}}=\mathcal{L}\phi_{\mathrm{n}}(x_{\mathrm{m}},y_{\mathrm{m}}), \ \mathrm{m}=1,\cdots,\mathrm{N_i}, \ \mathrm{n}=1,\cdots,\mathrm{N},$$
$$A_{\mathcal{B}_1}\in\mathbb{R}^{\mathrm{N_b}\times\mathrm{N}}, \quad \text{where} \quad (A_{\mathcal{B}_1})_{\ell,\mathrm{n}}=\mathcal{B}_1\phi_{\mathrm{n}}(x_{\mathrm{N_i}+\ell},y_{\mathrm{N_i}+\ell}), \ \ell=1,\cdots,\mathrm{N_b}, \ \mathrm{n}=1,\cdots,\mathrm{N},$$
$$A_{\mathcal{B}_2}\in\mathbb{R}^{\mathrm{N_b}\times\mathrm{N}}, \quad \text{where} \quad (A_{\mathcal{B}_2})_{\ell,\mathrm{n}}=\mathcal{B}_2\phi_{\mathrm{n}}(x_{\mathrm{N_i}+\ell},y_{\mathrm{N_i}+\ell}), \ \ell=1,\cdots,\mathrm{N_b}, \ \mathrm{n}=1,\cdots,\mathrm{N}.$$

To account for the second boundary condition we consider an additional $\mathrm{N_b}$ ghost points $\{(\mathrm{x_n},\mathrm{y_n})\}_{\mathrm{n}=\mathrm{N_i}+\mathrm{N_b}}^{\mathrm{N_i}+2\mathrm{N_b}}$. These additional ghost points can be viewed as a supplement

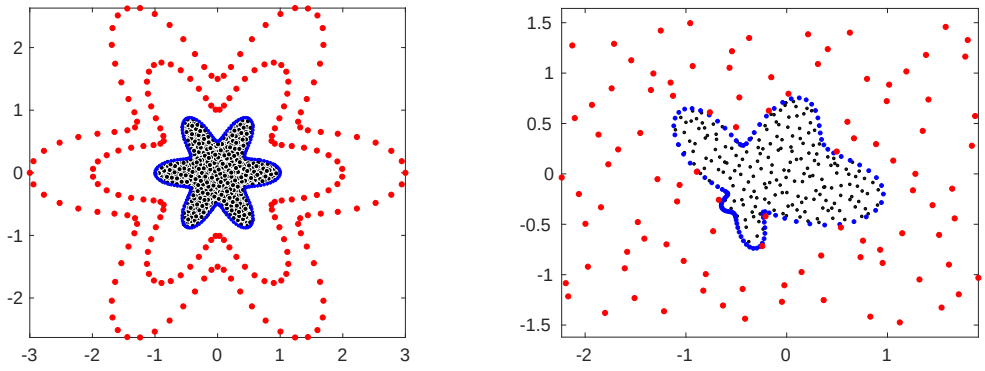

(a) (b)

Figure 1: The profiles of the distribution of interior points (black •), boundary points (blue •), and ghost points (red •).

of source points in analogy to the source points employed in another meshless method, namely, the MFS. The purpose of adding these points is to render linear system (2.9) square. With these additional ghost points, approximation (2.7) becomes

$$\hat{u}(x,y)=\sum_{n=1}^{N+N_b} a_n\phi_n(x,y), \qquad (x,y)\in\overline{\Omega}, \tag{2.10}$$

while (2.9) becomes a $(N+N_b)\times(N+N_b)$ linear system. As shall be demonstrated in the numerical tests, these ghost points, when appropriately spread inside and outside the domain, will significantly enhance the accuracy and stability of the RBFCMs. In Section 3, we will perform tests on how these ghost points should be distributed.

The ghost points may be distributed in various ways. In Fig. 1 we present two such distributions (also including the interior and boundary centres/collocation points). In Fig. 1(a) the ghost points are placed on two curves which are similar in shape to the boundary of the domain $\Omega$ while in Fig. 1(b) they are placed randomly in a square containing $\Omega$ but outside $\overline{\Omega}$. Note that the ghost points can be placed inside the domain as long as they do not coincide with the interior or boundary points.

### 2.2.2 The method of approximate particular solutions (MAPS)

In the MAPS [3], the approximation of the solution of BVP (2.6) is

$$\hat{u}(x,y)=\sum_{n=1}^{N} a_n\Psi_n(x,y), \qquad (x,y)\in\overline{\Omega}, \tag{2.11}$$

where

$$\Delta^2\Psi_n=\phi_n, \quad n=1,\cdots,N. \tag{2.12}$$

Note that in polar coordinates,

$$\Delta \equiv \frac{1}{r}\frac{d}{dr}\left(r\frac{d}{dr}\right) \text{ in 2D} \quad \text{and} \quad \Delta \equiv \frac{1}{r^2}\frac{d}{dr}\left(r^2\frac{d}{dr}\right) \text{ in 3D.}$$

In the case of the normalized inverse multiquadric (IMQ) ($\phi = 1/\sqrt{(cr)^2+1}$), by repeated integration and the process of de-singularization, we can obtain the closed-form particular solution $\Psi$ in (2.11) as follows [27]:

$$\Psi(r) = \begin{cases} \dfrac{4c^2r^2-11}{36c^4}\sqrt{1+c^2r^2} + \dfrac{2-3c^2r^2}{12c^4}\ln(1+\sqrt{1+c^2r^2}) + \dfrac{r^2}{4c^2}, & \text{in 2D,} \\ \begin{cases} \dfrac{2c^2r^2-13}{48c^4}\sqrt{1+c^2r^2} + \dfrac{4c^2r^2-1}{16c^5r}\sinh^{-1}(cr), & r \neq 0, \\ \dfrac{-1}{3c^4}, & r = 0, \end{cases} & \text{in 3D;} \end{cases} \tag{2.13}$$

and

$$\Phi(r) = \Delta\Psi(r) = \begin{cases} \dfrac{1}{c^2}(\sqrt{1+c^2r^2} - \ln(1+\sqrt{1+c^2r^2})), & \text{in 2D,} \\ \begin{cases} \dfrac{2\sqrt{1+c^2r^2}}{2c^2} + \dfrac{\sinh^{-1}(cr)}{2c^3r}, & r \neq 0, \\ \dfrac{1}{c^2}, & r = 0, \end{cases} & \text{in 3D.} \end{cases} \tag{2.14}$$

For the Neumann condition,

$$\frac{\partial\Psi(r)}{\partial n} = \big((x-\mathrm{x})n_x + (y-\mathrm{y})n_y\big)\frac{1}{r}\frac{\partial\Psi}{\partial r},$$

where $(n_x, n_y)$ is the unit normal vector at $(x,y)$ and $(\mathrm{x},\mathrm{y})$ is the centre point. By direct differentiation of (2.13), we obtain

$$\frac{1}{r}\frac{\partial\Psi(r)}{\partial r} = \begin{cases} \dfrac{1}{2c^2} + \dfrac{4c^2r^2-1}{12c^2\sqrt{1+c^2r^2}} + \dfrac{2\sqrt{1+c^2r^2}+2-c^2r^2}{12c^2\sqrt{1+c^2r^2}}\ln(1+\sqrt{1+c^2r^2}), & \text{in 2D,} \\ \begin{cases} \dfrac{c(2c^4r^4+r^2c^2-1)}{16c^5r^2\sqrt{1+r^2c^2}} + \dfrac{1+4c^2r^2}{16c^5r^3}\sinh^{-1}(cr), & r \neq 0, \\ 0, & r = 0, \end{cases} & \text{in 3D.} \end{cases} \tag{2.15}$$

Without loss of generality, let us assume

$$\mathcal{L} \equiv \Delta^2 + a\Delta + b\frac{\partial}{\partial x} + c\frac{\partial}{\partial y} + d, \tag{2.16}$$

where $a,b,c$ and $d$ are constants. From (2.7) and (2.11), we can see that the only difference between the two methods (Kansa method and MAPS) is the difference in the basis functions. In the same way as was done for the Kansa method, applying (2.11) to (2.6) and

(2.7), we obtain (2.9) where $A_{\mathcal{L}}, A_{\mathcal{B}_1}$, and $A_{\mathcal{B}_2}$ are now defined as follows:

$$A_{\mathcal{L}} \in \mathbb{R}^{\mathsf{N_i}\times\mathsf{N}}, \quad \text{where} \quad (A_{\mathcal{L}})_{\mathsf{m},\mathsf{n}} = \mathcal{L}\Psi_{\mathsf{n}}(x_{\mathsf{m}}, y_{\mathsf{m}}), \ \ \mathsf{m}=1,\cdots,\mathsf{N_i}, \ \ \mathsf{n}=1,\cdots,\mathsf{N}, \tag{2.17}$$

$$A_{\mathcal{B}_1} \in \mathbb{R}^{\mathsf{N_b}\times\mathsf{N}}, \quad \text{where} \quad (A_{\mathcal{B}_1})_{\ell,\mathsf{n}} = \mathcal{B}_1\Psi_{\mathsf{n}}(x_{\mathsf{N_i}+\ell}, y_{\mathsf{N_i}+\ell}), \ \ \ell=1,\cdots,\mathsf{N_b}, \ \ \mathsf{n}=1,\cdots,\mathsf{N}, \tag{2.18}$$

$$A_{\mathcal{B}_2} \in \mathbb{R}^{\mathsf{N_b}\times\mathsf{N}}, \quad \text{where} \quad (A_{\mathcal{B}_2})_{\ell,\mathsf{n}} = \mathcal{B}_2\Psi_{\mathsf{n}}(x_{\mathsf{N_i}+\ell}, y_{\mathsf{N_i}+\ell}), \ell=1,\cdots,\mathsf{N_b}, \mathsf{n}=1,\cdots,\mathsf{N}. \tag{2.19}$$

More specifically, from (2.12)-(2.14), (2.17) may be expressed as

$$\mathcal{L}\Psi = \phi + a\,\Phi + b\,\frac{\partial\Psi}{\partial x} + c\,\frac{\partial\Psi}{\partial y} + d\,\Psi.$$

As in (2.10) for the Kansa method, we add $\mathsf{N_b}$ ghost points and take

$$\hat{u}(x,y) = \sum_{\mathsf{n}=1}^{\mathsf{N}+\mathsf{N_b}} a_{\mathsf{n}}\Psi_{\mathsf{n}}(x,y), \qquad (x,y)\in\overline{\Omega}. \tag{2.20}$$

## 3 Numerical examples

In all numerical experiments in this section, we shall use the normalized inverse multiquadric (IMQ) $(1/\sqrt{(cr)^2+1})$ as the RBF in the Kansa method and its appropriate integrals in 2D and 3D in the MAPS. In RBF collocation methods, the determination of an appropriate value of the RBF shape parameter (when present) is a challenging issue and, as stated in Section 1, several attempts have been made to resolve it. In this section, we consider two such approaches, namely the LOOCV algorithm [29] and Franke's formula [12]. In 1982, Franke proposed to utilize the shape parameter value $c = D/(0.8\sqrt{N})$, where $D$ is the diameter of the smallest circle including all $N$ interpolation points, to approximate the optimal shape parameter value of the multiquadric RBF $(\sqrt{r^2+c^2})$. However, this formulation was proposed at a time when only single precision arithmetic was available. Later, Franke's formula was modified for double precision arithmetic to $c = D/(0.8N^{1/4})$. Note that for the normalized multiquadric (MQ) $(\sqrt{(cr)^2+1})$, Franke's formula should be the reciprocal of the MQ formula, that is $c = 0.8N^{1/4}/D$. Franke's formula was developed using MQ for scattered data interpolation. For the case of the Kansa method and the MAPS using IMQ, some modification of this formula is necessary. Based on extensive study and experimentation, we concluded that the value of the optimal shape parameter for the MAPS is usually larger than that for the Kansa method. Based on our numerical experiments, we revised Franke's formula by adding 1 for the MAPS and 0.5 for the Kansa method in all the numerical tests in this section. As we shall see in the following numerical examples, the modified Franke formula yields quite satisfactory results. We shall, therefore, be using this modified Franke formula as well as the LOOCV for selecting a good shape parameter for the IMQ. Note that each approach has its own merits. One of the disadvantages of the LOOCV is the computational cost. In the 2D case, the LOOCV works very well. However, in the 3D case, the computational cost becomes an issue.

After extensive experimentation, we found that the distribution of the ghost points can be quite arbitrary. In addition, we observed that if the ghost points were taken inside a circular disk in the 2D case and inside a sphere in the 3D case (in both cases containing the domain $\Omega$) a good estimate for the shape parameter of the IMQ using the modified Franke formula could be easily obtained. It should be noted that the ghost points should differ from the interior and boundary centre/collocation points. In the case when even one ghost point coincides with an interior or boundary centre/collocation point, the coefficient $(N+N_b)\times(N+N_b)$ matrix in system (2.9) becomes singular. To ensure that all the ghost points are fairly uniformly distributed, we employ the Halton quasi-random point generator which can be found in the MATLAB© command `haltonset`.

We calculated the approximate solution $\hat{u}$ at $L$ test points in $\overline{\Omega}$. and then calculated the maximum absolute error $E$ given by

$$E=||u-\hat{u}||_{\infty,\overline{\Omega}}. \tag{3.1}$$

**Example 3.1.** We consider the fourth order BVP (2.6) in the 2D amoeba-shaped domain depicted in Fig. 2(a) and described parametrically by

$$\Omega=\left\{(x,y):x=\frac{1}{2}r(\vartheta)\cos\vartheta-\frac{2}{5},y=\frac{1}{2}r(\vartheta)\sin\vartheta-\frac{1}{5},\ 0\leq\vartheta\leq2\pi\right\},$$

where

$$r(\vartheta)=e^{\sin\vartheta}\sin^2(2\vartheta)+e^{\cos\vartheta}\cos^2(2\vartheta). \tag{3.2}$$

In (2.6), $\mathcal{L}\equiv\Delta^2$ and $f(x,y)$,$g(x,y)$, and $h(x,y)$ are derived from the exact solution

$$u(x,y)=\frac{4}{4+x+y},$$

the profile of which is shown in Fig. 2(b).

First, we consider the so-called *second biharmonic problem* where $\mathcal{B}_1\equiv I,\mathcal{B}_2\equiv\Delta$. In our numerical experiments, we took $N_b=300,N_i=400$, and $L=100$, respectively. The 300 ghost points are distributed randomly inside the circle with center at $(0.4,0.2)$ and radius $R=4$. In Fig. 3(a), we present the absolute errors versus $c$ for the two RBF collocation methods studied in this paper. From this figure, it appears that the MAPS is more stable than the Kansa method which is more sensitive to changes in the values of the shape parameter. The acceptable "good interval" range for the shape parameter of the Kansa method is narrower than that of the MAPS. As far as the optimal accuracy is concerned, there is little to choose between the two approaches. In contrast, from Fig. 3(b), we observe that the accuracy of the two approaches for the same number of interior and boundary points without ghost points is considerably lower. In particular, the Kansa method is highly unstable with respect to the change of the shape parameter. With the introduction of the ghost points, the stability of the Kansa method improves. For these two approaches, the addition of more interior and boundary points (still without ghost points) does not improve the accuracy as shown in Fig. 3(b).

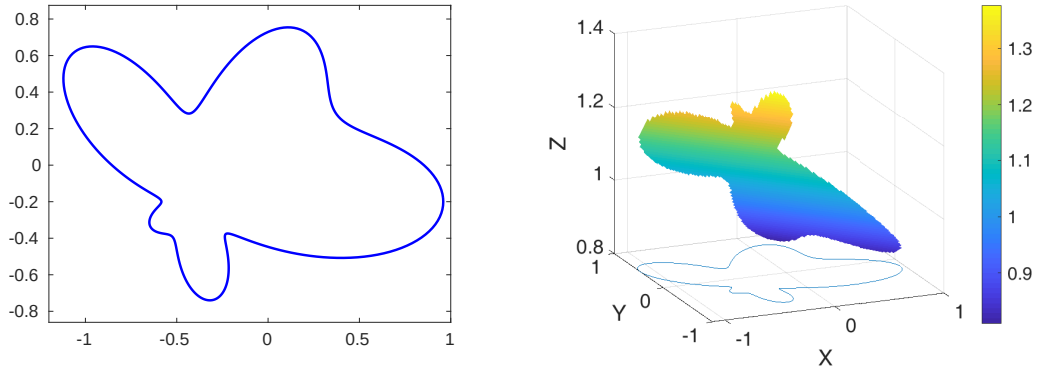


(a) (b)

Figure 2: Example 3.1: The profiles of (a) amoeba-shaped domain; (b) exact solution.

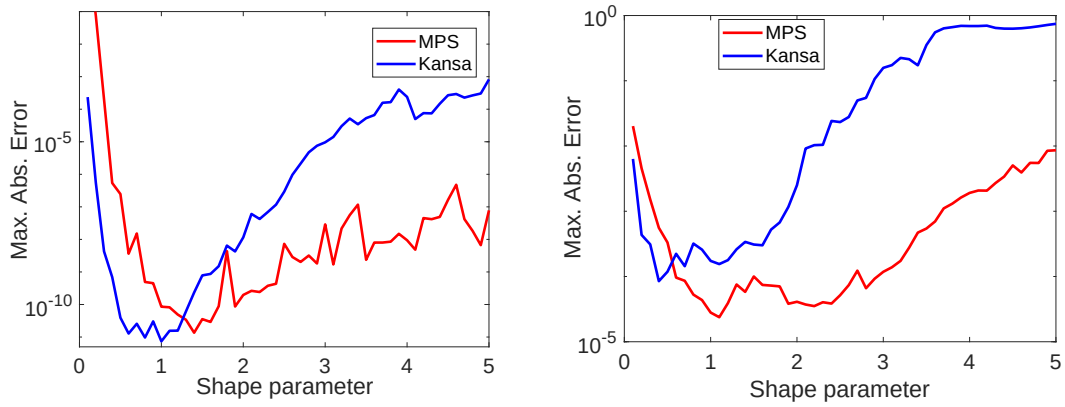


(a) (b)

Figure 3: Example 3.1: The maximum absolute errors versus the shape parameter (a) using the ghost points; (b) without the ghost points.

In Table 1, we present the maximum absolute errors of the two methods using LOOCV for obtaining a good value for the shape parameter. To apply LOOCV, we need to provide an initial search interval $[c_{\min},c_{\max}]$. The results indicate that the Kansa method is slightly more accurate than the MAPS. The reason for this could be the fact that, as Fig. 3 indicates, the error profile of the Kansa method is more stiff and it is therefore easier for the search algorithm to identify the minimum. As a consequence, the apparent disadvantage of the Kansa method has turned into an advantage when using LOOCV, to identify the minimum error. We also employed the modified Franke formula to obtain an approximation of the optimal shape parameter. The results of Table 2 indicate that the results obtained using the modified Franke formula are comparable to those ob-

Table 1: Example 3.1: Maximum absolute errors and the optimal shape parameter $c$ using LOOCV with initial search interval $[c_{\min},c_{\max}]$ and Franke's formula with $R=4$.

| $[c_{\min},c_{\max}]$ | $c$ | Kansa | $c$ | MAPS |
|---|---|---|---|---|
| [0.3,3] | 1.038 | 2.694(-12) | 1.020 | 1.137(-10) |
| [0.3,4] | 1.304 | 2.051(-11) | 1.276 | 7.494(-11) |
| [0.3,5] | 0.935 | 2.720(-12) | 1.748 | 3.211(-10) |
| [0.3,6] | 1.132 | 5.781(-12) | 1.387 | 5.531(-11) |
| Franke [12] | 1.062 | 2.102(-12) | 1.562 | 8.181(-11) |

Table 2: Example 3.1: Maximum absolute errors and the shape parameters using the modified Franke formula for various radii of the ghost disk.

| $R$ | $c$ | Kansa | $c$ | MAPS |
|---|---|---|---|---|
| 3 | 1.250 | 1.245(-8) | 1.750 | 5.063(-11) |
| 4 | 1.062 | 1.802(-11) | 1.562 | 8.181(-11) |
| 5 | 0.950 | 1.878(-11) | 1.450 | 2.899(-10) |
| 6 | 0.875 | 1.787(-11) | 1.375 | 1.704(-10) |

tained with LOOCV in terms of accuracy. Clearly, the approach using Franke's formula is computationally much more efficient than LOOCV.

Another important issue in the distribution of the ghost points is how far the circular disk of radius, say, $R$, containing them should be extended beyond the domain. In Table 2, for the results which are obtained using the modified Franke formula, we observe that the accuracy of both methods is fairly high. In particular, for the Kansa method, the larger the ghost disk the better. In contrast, for the MAPS, a smaller ghost disk produces better results. An interesting observation is that if we move all the ghost points inside the domain, then the accuracy drops considerably to the range of $10^{-4}\sim10^{-5}$ for both methods. On the other hand, if we move the ghost points outside the domain and take no ghost points inside, then little difference is observed in terms of accuracy. Furthermore, when the ghost disk is too small, say $R<1.5$, then the accuracy of both methods drops to the level of the traditional method. Hence, placing the ghost points far enough outside the domain is critical to the improvement of the performance of both methods.

We also conducted tests investigating the effect of the size of the ghost circle on the condition number of the coefficient matrix in the Kansa method. As shown in Table 3, the condition numbers remain approximately the same for various radii of the ghost circle. According to the Principle of Uncertainty by Schaback [30], the high condition number in RBF collocation methods is not an issue as long as the condition number stays within the tolerance of the machine precision before it breaks down.

Next, we consider so-called *first biharmonic problem* where $\mathcal{B}_1\equiv I,\mathcal{B}_2\equiv\partial/\partial n$ and also the case $\mathcal{B}_1\equiv I,\mathcal{B}_2\equiv\partial^2/\partial n^2$. The same collocation points and $R=4$ are used. Here we consider the Kansa method with LOOCV. Note that for the second Neumann condition

Table 3: The condition numbers for various radii of ghost circle.

| $D$ | condition # | Maximum absolute error |
|---|---|---|
| 3 | 1.0406e+21 | 1.245e-08 |
| 4 | 1.4120e+22 | 2.102e-12 |
| 5 | 5.5613e+20 | 1.878e-11 |
| 6 | 1.4134e+22 | 1.787e-11 |
| 7 | 3.8902e+21 | 4.959e-11 |
| 8 | 1.9960e+21 | 2.913e-10 |
| 9 | 5.4196e+21 | 6.246e-10 |

Table 4: Example 3.1: Maximum absolute errors and the optimal shape parameter $c$ using the Kansa method with LOOCV and Franke's formula for $R=4$.

| | $\mathcal{B}_1\equiv I$, | $\mathcal{B}_2\equiv\partial/\partial n$ | $\mathcal{B}_1\equiv I$, | $\mathcal{B}_2\equiv\partial^2/\partial n^2$ |
|---|---|---|---|---|
| $[c_{\min},c_{\max}]$ | $c$ | $E$ | $c$ | $E$ |
| [0.3,2] | 0.752 | 3.897(-09) | 0.725 | 1.736(-12) |
| [0.3,3] | 0.937 | 1.705(-12) | 0.445 | 1.249(-09) |
| [0.3,4] | 3.127 | 4.071(-08) | 2.549 | 1.717(-09) |
| [0.3,5] | 3.181 | 9.553(-08) | 2.126 | 6.502(-10) |
| Franke [12] | 1.062 | 2.853(-13) | 1.062 | 3.693(-11) |

$\mathcal{B}_2\equiv\partial^2/\partial n^2$, we have

$$\begin{aligned}\frac{\partial^2\phi}{\partial n^2}&=\frac{\partial}{\partial n}(\phi_x n_x+\phi_y n_y)\\&=\phi_{xx}n_x^2+2\phi_{xy}n_x n_y+\phi_{yy}n_y^2,\end{aligned}$$

where $(n_x,n_y)$ is the unit normal vector at $(x,y)$, (x,y) is the centre point and

$$\begin{aligned}\phi_{xx}&=(x-\mathrm{x})\frac{3c^4}{(1+r^2c^2)^{5/2}}-\frac{c^2}{(1+r^2c^2)^{3/2}},\\\phi_{xy}&=(x-\mathrm{x})(y-\mathrm{y})\frac{3c^4}{(1+r^2c^2)^{5/2}},\end{aligned}$$

and $\phi_{yy}$ can be obtained by replacing $(x-\mathrm{x})$ by $(y-\mathrm{y})$ in $\phi_{xx}$. The results shown in Table 4 remain highly accurate. In this table, we also present the results using the modified Franke formula for selecting the MQ shape parameter. We observe that the modified Franke formula yields a better prediction for a good shape parameter than LOOCV.

**Example 3.2.** We now consider the first biharmonic problem (2.6) with $\mathcal{B}_1\equiv I$, $\mathcal{B}_2\equiv\partial/\partial n$ in the 3D Stanford Bunny domain depicted in Fig. 4. The boundary points and the corresponding normals can be found at the website of the Stanford Computer Graphics Laboratory [39]. In our implementation, the size of the original Bunny is magnified tenfold.

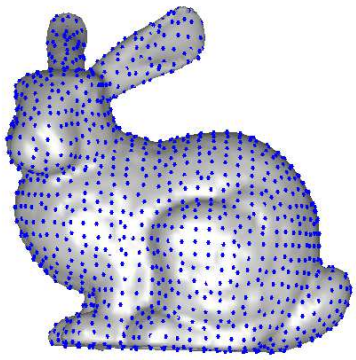

Figure 4: Example 3.2: The profile of the Stanford Bunny domain with 1877 boundary points.

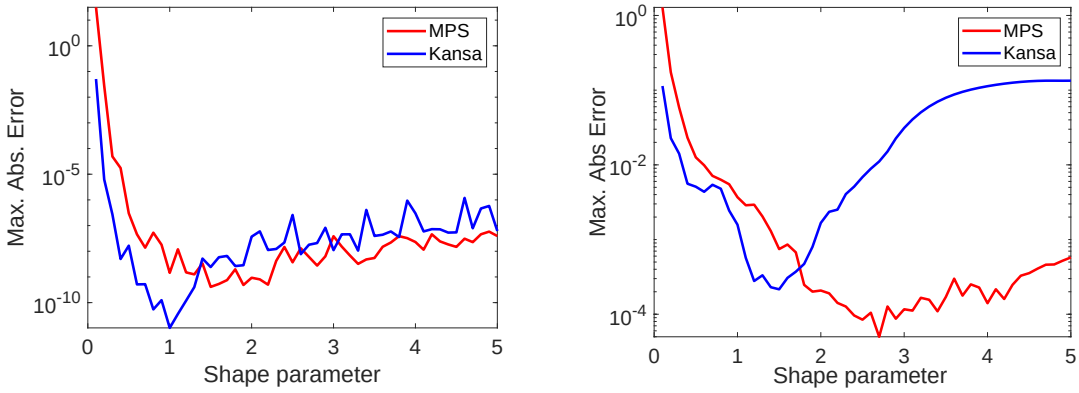


Figure 5: Example 3.2: The maximum absolute errors versus the shape parameter (a) using the ghost points and (b) without the ghost points.

In (2.6), $\mathcal{L}\equiv\Delta^2$ and $f(x,y,z)$,$g(x,y,z)$ and $h(x,y,z)$ are derived from the exact solution

$$u(x,y)=\frac{1}{120}(x^5+y^5+z^5)+\mathrm{e}^{x+y+z}. \tag{3.3}$$

We took $\mathrm{N_b}=1877,\mathrm{N_i}=1000$, and $L=500$ and the 1877 ghost points are distributed randomly inside the sphere with center $(-0.1683,1.0866,0)$ and radius $R=4$. In Fig. 5, we present the maximum absolute errors versus the shape parameter $c$ when using and when not using ghost points with both the Kansa method and the MAPS. It is evident that the accuracy when using ghost points is much higher than when using the traditional method without them. Furthermore, when not using ghost points, the MAPS is superior to the Kansa method in terms of both accuracy and stability. When using ghost points, the

Table 5: Example 3.2: Maximum absolute errors and the optimal shape parameter $c$ using LOOCV with initial search interval $[c_{\min},c_{\max}]$.

| $[c_{\min},c_{\max}]$ | $c$ | Kansa | $c$ | MAPS |
|---|---|---|---|---|
| [0.3,2] | 0.949 | 2.281(-11) | 0.949 | 1.675(-08) |
| [0.3,3] | 0.698 | 8.080(-11) | 1.331 | 6.832(-10) |
| [0.3,4] | 0.856 | 3.285(-11) | 1.713 | 5.477(-10) |
| Franke | 1.330 | 4.141(-10) | 1.830 | 2.973(-09) |

Kansa method becomes as stable as and more accurate than the MAPS if we can identify the optimal shape parameter.

Next, we investigate the determination of a good value for shape parameter. In Table 5, we present the maximum absolute errors using the LOOCV for the determination of an appropriate shape parameter. As there are now many more collocation points, the use of LOOCV is very time-consuming. In contrast, the modified Franke formula also provides a very good estimate for the shape parameter without compromising the computational cost of the method. It is clear that the performance of the Kansa method is superior to that of the MAPS, which is consistent with the results shown in Fig. 5(a).

**Example 3.3.** We finally consider a 3D BVP where, in (2.6), $\mathcal{L}\equiv\Delta^2+\alpha\Delta+\beta$ and $\mathcal{B}_1\equiv I$, $\mathcal{B}_2\equiv\Delta$. The given functions $f$,$g$ and $h$ in (2.6) are derived from the exact solution $u(x,y,z)=e^{x+y+z}$, $\alpha$ and $\beta$ are constants, and the domain $\Omega$ is a 3D propeller, the profile of which is shown in Fig. 6(a).

In the numerical implementation, we chose $N_b=2053$ (see Fig. 6(b)), $N_i=1500$, and $L=500$. The 2053 ghost points are distributed randomly inside the sphere with center $(0.325,1.225,1.220)$ and radius 4. In Fig. 7, we present the absolute maximum errors ver-

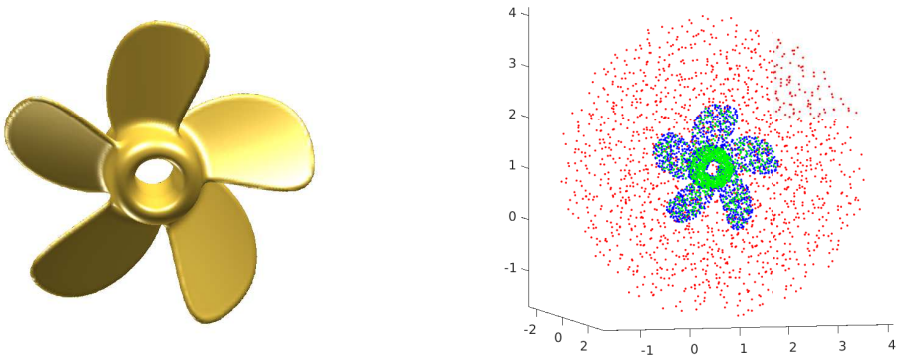


(a) (b)

Figure 6: Example 3.3: The profiles of the 3D (a) propeller domain and (b) 2053 boundary points (blue •), 1500 interior points (green •), and 2053 ghost points (red •).

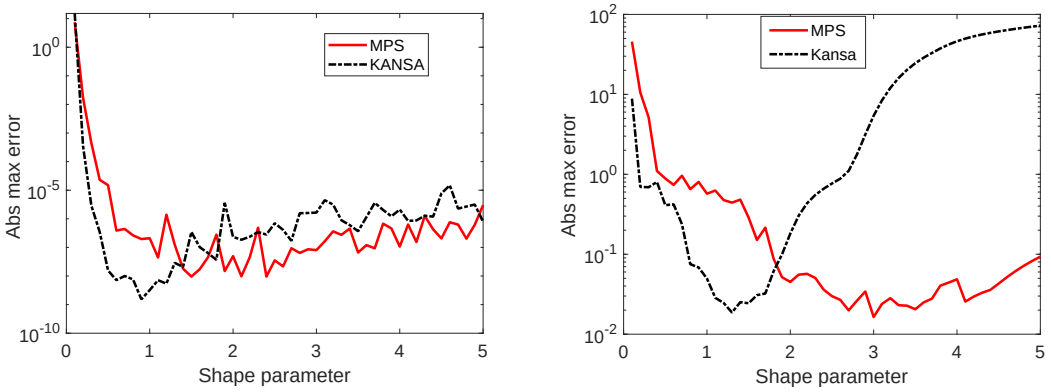


(a) (b)

Figure 7: Example 3.3: The absolute maximum error for the case $\alpha=\beta=60$: (a) with ghost points; (b) without ghost points.

Table 6: Example 3.3: Maximum absolute errors for various $\alpha$ and $\beta$.

| | | Kansa method | MAPS |
|---|---|---|---|
| $\alpha$ | $\beta$ | $c=1.365$ | $c=1.865$ |
| 1 | 1 | 1.058(-8) | 1.783(-8) |
| 20 | 20 | 1.210(-7) | 7.099(-8) |
| 40 | 40 | 2.807(-8) | 5.383(-8) |
| 60 | 60 | 1.222(-8) | 3.336(-8) |

sus the shape parameter when $\alpha=\beta=60$, with and without the ghost points. As was the case in the 2D Example 3.1, there is a considerable difference between Figs. 7(a) and 7(b) in terms of accuracy. Furthermore, we observe that the gap between the MAPS and the Kansa method in Fig. 7(a) is much smaller than in Fig. 7(b). This implies that the presence of the ghost points is important in stabilizing the solution of the Kansa method with respect to the shape parameter. With the ghost points, the Kansa method becomes not only more stable but also more accurate than the MAPS if we can identify the optimal value of the shape parameter.

In this example, we do not use LOOCV for the determination of the shape parameter of IMQ since the system matrix is fairly large and the search algorithm becomes too expensive. In Table 6, we present the absolute maximum errors for various values of $\alpha$ and $\beta$ with the same number of collocation and ghost points using the Kansa method and the MAPS with the modified Franke formula for the approximation of the shape parameter. We observe that the results remain highly accurate for different values of $\alpha$ and $\beta$.

We next explore the impact of the size of the sphere of radius, say, $R$, containing the ghost points. Considering the case $\alpha=\beta=60$, in Table 7 we observe that the MAPS yields better accuracy for small $R$ while the Kansa method performs better for larger $R$. This

Table 7: Example 3.3: Maximum absolute errors for various sizes of the ghost sphere in the case $\alpha=\beta=60$.

| $R$ | $c$ | Kansa method | $c$ | MAPS |
|---|---|---|---|---|
| 3 | 1.654 | 7.191(-8) | 2.154 | 6.452(-9) |
| 4 | 1.365 | 1.222(-8) | 1.865 | 3.336(-8) |
| 5 | 1.192 | 3.359(-8) | 1.692 | 1.158(-7) |
| 6 | 1.077 | 4.703(-9) | 1.577 | 1.343(-7) |

result is consistent with the corresponding results for the 2D Example 3.1. Hence, we conclude that when using the modified Franke formula, for the MAPS we should choose a smaller ghost sphere while for the Kansa method we should take a larger ghost sphere.

**Example 3.4.** To further demonstrate the effectiveness of the proposed method, we consider the following Kirchhoff thin plate problem [36] in a polygonal domain for which no exact solution is available:

$$\begin{aligned}
&\Delta^2 u(x,y)=\frac{q}{D}, \quad (x,y)\in\Omega,\\
&u(x,y)=0, \quad (x,y)\in\partial\Omega,\\
&\frac{\partial}{\partial n}u(x,y)=0, \quad (x,y)\in\partial\Omega,
\end{aligned}$$

where $u(x,y)$ is the deflection of the thin plate, $q=10^6$ is the constant transverse load, $D=Eh^3/(12(1-\mu^2))$ is the flexural rigidity, $E=2.1\times10^{11}$ is the elastic modulus of steel, $h=0.01$ is the thickness of the plate, and $\mu=0.3$ is Poisson's ratio for steel. The profile of the polygonal domain is shown in Fig. 8(a).

In the numerical implementation, we chose $\mathsf{N_b}=345$, $\mathsf{N_i}=317$, and for this example, we only consider the Kansa method. The radius of the ghost circle is set to 4 and its center is the geometric center of the polygon. For the selection of the shape parameter, we used the modified Franke formula as described in the previous examples. The profile of the approximate solution is shown in Fig. 8(b) which is not as accurate as one would have expected. However, when we solve the linear system using singular value decomposition (SVD) (with cut-off singular value $10^{-10}$), we obtain a much improved solution profile as shown in Fig. 9(a). For convenience, the MATLAB© command `pinv` (Moore-Penrose pseudoinverse) is used for this purpose. In contrast, with the traditional Kansa method and the modified Franke formula (without adding 0.5) for the shape parameter, we obtain the approximate solution shown in Fig. 9(b). No further improvement is observed when using `pinv` or adjusting the different shape parameters. Clearly, the approximate solution on the boundary is problematic.

Since no exact solution is available, we compare our results with those obtained using the finite element method (FEM) commercial package COMSOL Multiphysics© [5]. The COMSOL approximate solution was obtained with 5582 elements. The profile of the error between the proposed method and the FEM solution is presented in Fig. 10. Note that for various radii of the ghost circle, results similar to those shown above were obtained.

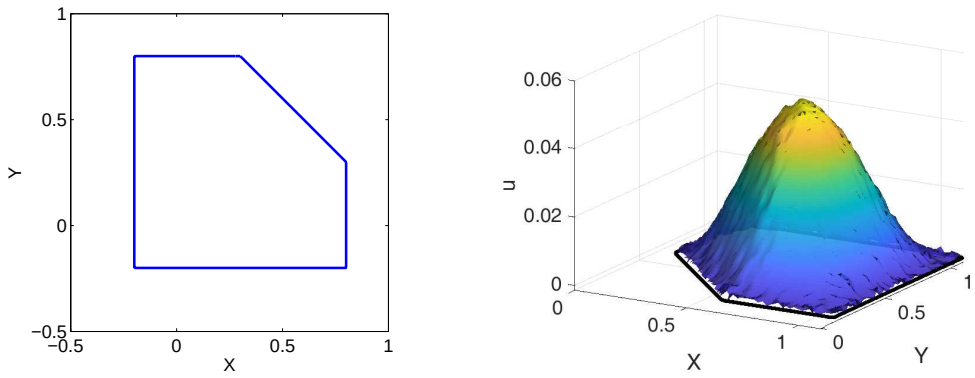


(a) (b)

Figure 8: Example 3.4: The profiles of (a) the polygonal domain and (b) the approximate solution.

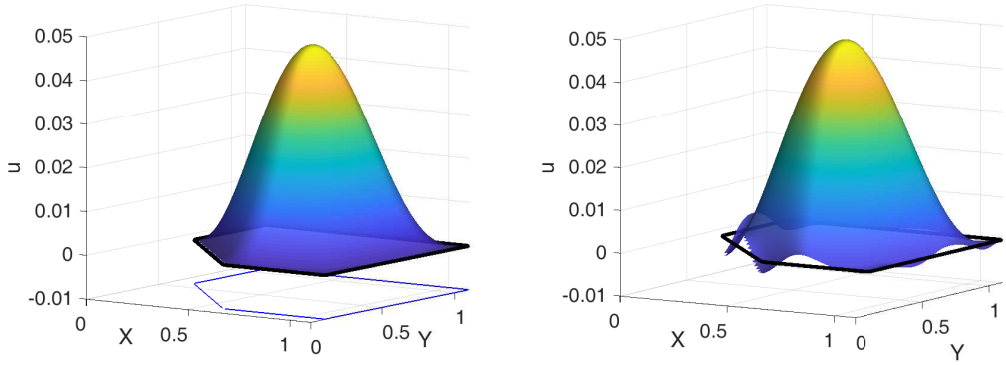


(a) (b)

Figure 9: Example 3.4: The profiles of the approximate solution using (a) ghost points and SVD and (b) the traditional Kansa method.

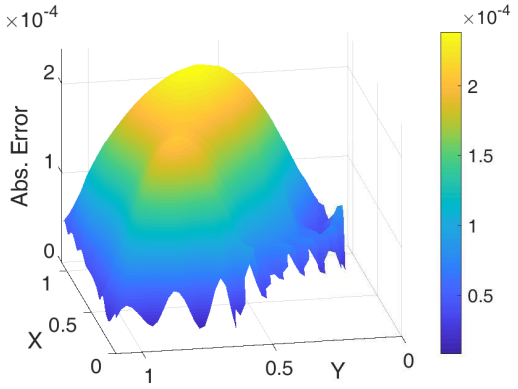


Figure 10: Example 3.4: The profile of the absolute error with respect to the results obtained using COMSOL.

# 4 Conclusions

We have investigated the application of two RBF collocation methods to fourth order BVPs. In particular, we propose new formulations for the Kansa method and the MAPS when these are applied to fourth order problems in which, to compensate for the second boundary condition, we introduce a number of so-called ghost points. These points are located in a circular disk (2D problems) or a sphere (3D problems) containing the domain of the problem under investigation. Their number is equal to the number of boundary centres/collocation points in the classical RBF discretization, which yields a square linear system. The addition of the ghost points is somehow analogous to the presence of the source points in another meshless method, the MFS. The determination of the RBF shape parameter in the methods used is achieved using either the LOOCV algorithm or a modification of Franke's formula. For 2D problems the LOOCV algorithm is preferred, while for 3D problems, for computational cost considerations, Franke's formula is applied. The results of several computational tests in 2D and 3D revealed that the inclusion of the ghost points to the RBF discretization improves both the accuracy and the stability of the two collocation methods investigated. In the traditional approach, the stability and accuracy of the MAPS is better than that of the Kansa method. The addition of the ghost points, not only improves the accuracy of the Kansa method but also its stability. As a result, the Kansa method becomes the method of choice for solving BVPs governed by fourth order PDEs. The main element of originality of the current paper is the introduction of the ghost points spreading outside the domain. We also carry out a thorough investigation for the selection of a good shape parameter of the IMQ and a proper choice of the ghost disk/sphere in 2D/3D.

In future work we intend to study the optimal placement of the ghost points and also the application of the current formulation to other types of PDEs and other RBF-related collocation methods such as the RBF-differential quadrature method [32].

# Acknowledgments

The first author acknowledges HPC at the University of Southern Mississippi supported by the National Science Foundation under the Major Research Instrumentation (MRI) program via Grant # ACI 1626217. The third author is supported by National Natural Science Foundation (No. 11702125), Post-doctor Program (No. 208006) of China grant and Double Thousand Talents Project from Jiangxi Province.

### References

[1] Y. Bai, Y. Wu and X. Xie, Uniform convergence analysis of a higher order hybrid stress quadrilateral finite element method for linear elasticity, Adv. Appl. Math. Mech., 8(2016), 399–425.

[2] Y. Bai, Y. Wu and X. Xie, Superconvergence and recovery type a posteriori error estimation for hybrid stress finite element method, Sci. China Math., 59(2016), 1835–1850.
[3] C. S. Chen, C. M. Fan and P. H. Wen, The method of particular solutions for solving certain partial differential equations, Numer. Methods Partial Differential Equations, 28(2012), 506–522.
[4] C. S. Chen and A. Karageorghis, Local RBF algorithms for elliptic boundary value problems in annular domains, Commun. Comput. Phys., 25(2019), 41–67.
[5] COMSOL Multiphysics® v. 5.2. www.comsol.com, COMSOL AB, Stockholm, Sweden.
[6] E. Divo and A. J. Kassab, An efficient localized RBF meshless method for fluid flow and conjugate heat transfer, J. Heat Trans.-T. ASME, 129(2007), 124–136.
[7] G. Fairweather and A. Karageorghis, The method of fundamental solutions for elliptic boundary value problems, Adv. Comput. Math., 9(1998), 69–95.
[8] G. E. Fasshauer, Solving partial differential equations by collocation with radial basis functions, in Surface Fitting and Multiresolution Methods, A. Le Méhauté, C. Rabut, and L. L. Schumaker (eds.), Vanderbilt University Press (Nashville, TN), pp. 131–138, 1997.
[9] G. E. Fasshauer, Meshfree Approximation Methods with MATLAB, Interdisciplinary Mathematical Sciences, vol. 6, World Scientific Publishing Co. Pte. Ltd., Hackensack, NJ, 2007.
[10] G. E. Fasshauer and J. G. Zhang, On choosing optimal shape parameters for RBF approximation, Numer. Algorithms, 45(2007), 345–368.
[11] N. Flyer, G. A. Bernett and L. J. Wicker, Enhancing finite differences with radial basis functions: experiments on the Navier-Stokes equations, J. Comput. Phys., 316(2016), 39–62.
[12] R. Franke, Scattered data interpolation: tests of some methods, Math. Comp., 38(1982), 181–200.
[13] Z. Fu and W. Chen, A truly boundary–only meshfree method applied to Kirchhoff plate bending problems, Adv. Appl. Math. Mech., 1(2009), 341–352.
[14] M. A. Golberg and C. S. Chen, The method of fundamental solutions for potential, Helmholtz and diffusion problems, Boundary Integral Methods: Numerical and Mathematical Aspects (M. A. Golberg, ed.), Comput. Eng., vol. 1, WIT Press/Comput. Mech. Publ., Boston, MA, 1999, pp. 103–176.
[15] D. Halpern, O. E. Jensen and J. B. Grotberg, A theoretical study of surfactant and liquid delivery into the lung, J. Appl. Physiol., 85(1998), 333–352.
[16] M. A. Jankowska, A. Karageorghis and C. S. Chen, Improved Kansa RBF method for the solution of nonlinear boundary value problems, Eng. Anal. Bound. Elem., 87(2018), 173–183.
[17] E. J. Kansa, Multiquadrics—a scattered data approximation scheme with applications to computational fluid-dynamics. II. Solutions to parabolic, hyperbolic and elliptic partial differential equations, Comput. Math. Appl., 19(1990), 147–161.
[18] E. J. Kansa and Y. C. Hon, Circumventing the ill-conditioning problem with multiquadric radial basis functions: applications to elliptic partial differential equations, Comput. Math. Appl., 39(2000), 123–137.
[19] A. Karageorghis, C. S. Chen and X.-Y. Liu, Kansa-RBF algorithms for elliptic problems in axisymmetric domains, SIAM J. Sci. Comput., 38(2016), A435–A470.
[20] E. Larsson and B. Fornberg, A numerical study of some radial basis function based solution for elliptic PDEs, Comput. Math. Appl., 46(2003), 891–902.
[21] C. K. Lee, X. Liu and S. C. Fan, Local multiquadric approximation for solving boundary value problems, Comput. Mech., 30(2003), 396–409.
[22] J. Li, F. Liu, L. Feng and I. Turner, A novel finite volume method for the Riesz space

distributed-order advection-diffusion equation, Appl. Math. Model., 46(2007), 536–553.
[23] J. Li, F. Liu, L. Feng and I. Turner, A novel finite volume method for the Riesz space distributed-order diffusion equation, Comput. Math. Appl., 74(2017), 772–783.
[24] S. Li and L. Ling, Collocation methods for Cauchy problems of elliptic operators via conditional stabilities, Commun. Comput. Phys., 26(2019), 785–808.
[25] F. Liu, L. Feng, V. Anh and J. Li, Unstructed-mesh Galerkin finite element method for the two-dimensional multi-term time-space fractional Bloch-Torrey equations on irregular convex domains, Comput. Math. Appl., 78(2019), 1637–1650.
[26] X.-Y. Liu, A. Karageorghis and C. S. Chen, A Kansa-radial basis function method for elliptic boundary value problems in annular domains, J. Sci. Comput., 65(2015), 1240–1269.
[27] J. Monroe, Hybrid meshless method for numerical solution of partial differential equations, Ph.D. Dissertation, University of Southern Mississippi, 2014.
[28] M. J. D. Powell, Radial basis function methods for interpolation to functions of many variables, DAMTP Report NA11, University of Cambridge, Cambridge, UK, 2001.
[29] S. Rippa, An algorithm for selecting a good value for the parameter *c* in radial basis function interpolation, Adv. Comput. Math., 11(1999), 193–210.
[30] R. Schaback, On the efficiency of interpolation by radial basis functions, in Surface Fitting and Multiresolution Methods, A. Le Méhauté, C. Rabut, and L.L. Schumaker (eds.), Vanderbilt University Press, (Nashville, TN), pp. 309-318, 1997.
[31] A. Safdari-Vaighani, E. Larsson and A. Heryudono, Radial basis function methods for the Rosenau equation and higher order PDEs, J. Sci. Comput., 75(2018), 1555–1580.
[32] C. Shu and Y. L. Wu, Integrated radial basis functions-based differential quadrature method and its performance, Int. J. Numer. Meth. Fluids, 53(2007), 969–984.
[33] R. Tankelevich, G. Fairweather and A. Karageorghis, Three dimensional image reconstruction using the PF/MFS technique, Eng. Anal. Bound. Elem., 33(2009), 1403–1410.
[34] S. Vong, P. Lyu and Z. Wang, A compact difference scheme for fractional sub-diffusion equations with the spatially variable coefficient under Neumann boundary conditions, J. Sci. Comput., 66(2016), 725–739.
[35] H. Y. Wu and Y. Duan, Multi-quadric quasi-interpolation method coupled with FDM for the Degasperis-Procesi equation, Appl. Math. Comput., 274(2016), 83–92.
[36] J. Xiong, P. Jiang, H. Zheng and C. S. Chen, A high accurate simulation of thin plate problems by using the method of approximate particular solutions with high order polynomial basis, Eng. Anal. Bound. Elem., 94(2018), 153–158.
[37] G. Yao, C. S. Chen and H. Zheng, A modified method of approximate particular solutions for solving linear and nonlinear PDEs, Numer. Methods Partial Differential Equations, 33(2017), 1839–1858.
[38] G. Yao, J. Kolibal and C. S. Chen, A localized approach for the method of approximate particular solutions, Comput. Math. Appl., 61(2011), 2376–2387.
[39] `http://graphics.stanford.edu/data/3Dscanrep/`